

Fig. 2—Michelson interferometers with corner mirrors. H = horn, CM = corner mirror, BS = beam splitter.

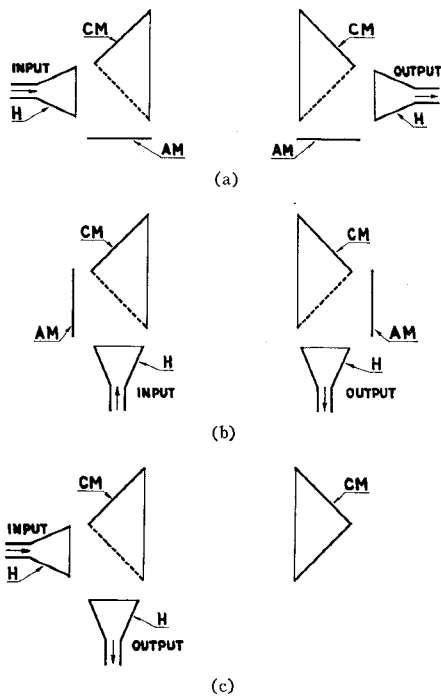


Fig. 3—Fabry-Perot interferometer variants with corner mirrors. H = horn, CM = corner mirror, AM = absorption mat.

absorption mats, without which the interferometer operation could be disturbed. The set in Fig. 3(b) has the horn axes situated parallel to one another. The variant in Fig. 3(c) is a further Fabry-Perot interferometer modification. Of course, in Figs. 3(b) and (c), a suitable setting of perforated plane mirror with respect to the horn is required.

A Fabry-Perot interferometer with corner mirrors possesses, besides previously mentioned insensitivity against misalignment, increased ruggedness—another valuable property. In this set there are no possibilities of the existence of unwanted multiple reflections in the space horn-mirror, since the corner mirror reflects onto the sides the waves falling on it from the back.

One could also apply in ultramicrowave interferometers, total internal reflection prisms, instead of metallic corner mirrors as was proposed with respect to lasers.⁵ However, the available dielectric materials limit this scheme to rather lower Q cavities.

⁵ Z. Godziński, "Application of total internal reflection prism for gaseous lasers," *PROC. IEEE (Correspondence)*, vol. 51, p. 361; February, 1963.

In the author's opinion, the application of corner mirrors for ultramicrowave interferometers instead of planar or spherical mirrors should simplify considerably the construction and improve the ruggedness of these instruments. It will also enable achievement of new constructional solutions.

The author would like to thank Prof. M. Suski and Prof. Z. Godziński for their useful and helpful discussions.

M. KŁOZA
Radio Dept.
Polytechnic Inst. Wrocław
Wrocław, Poland

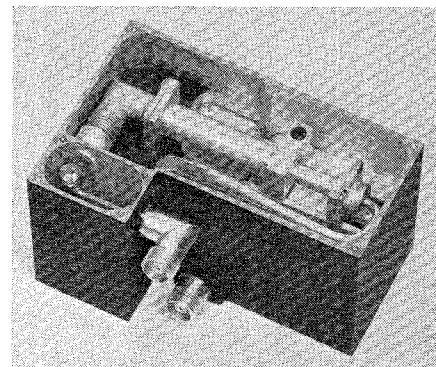


Fig. 1—X16 varactor multiplier in prototype package.

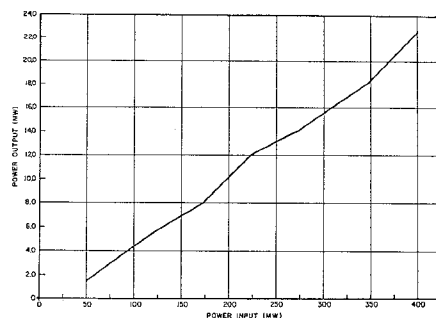


Fig. 2—Plot of typically obtained power output vs power input ($f_0 = 5650$ Mc).

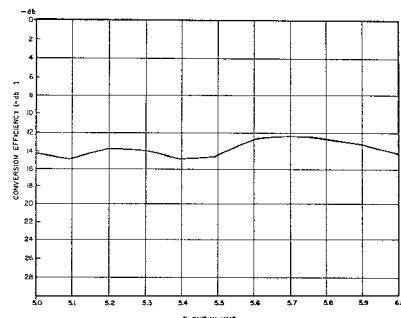


Fig. 3—X16 varactor multiplier tuned over a 1-kMc frequency range. Resulting increase in conversion loss is less than 3 db.

Manufacturers. The diodes can be operated either with self bias or fixed dc bias.

The X16 varactor multiplier is shown in prototype package in Fig. 1. A plot of power output vs power input typically obtained is shown in Fig. 2. The multiplier has been tuned over a 1-kMc frequency range with a resultant increase in conversion loss of less than 3 db. This is shown in the curve of conversion efficiency plotted in Fig. 3. The instantaneous bandwidth of the multiplier is approximately 20 Mc over this 1-kMc tuning range. Both the instantaneous bandwidth and the tuning range are limited by characteristics of the output band-pass filter rather than by the varactor multiplier.

As part of a missile-borne system, the varactor multiplier has been subjected to severe environmental tests. It is capable of withstanding vibration of 20 g's in three planes, from 20–2000 cps (maximum double

* Received September 13, 1963.

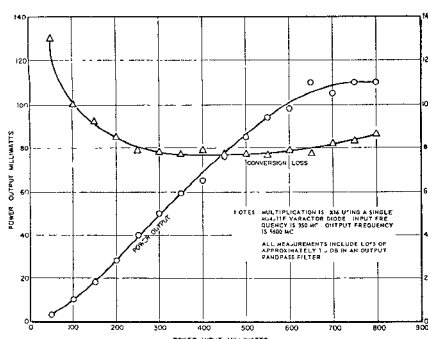


Fig. 4—Efficiency vs drive as obtained with a selected MS4511F diode.

excursion of 0.5 inch), with no change in electrical performance. Power variation for a temperature change from 25°C to 70°C averages ± 0.7 db with an additional power drop of 1.3 db up to 100°C. The power output, however, remains constant from 0°C to 25°C.

While these results are typical, substantially higher efficiencies have been obtained with specially selected diodes. Conversion losses as low as 7.7 db, including a 1.5-db output-filter loss, have been repeatedly achieved. A plot of efficiency vs drive obtained with a MS4511F diode is shown in Fig. 4.

The authors thank W. Venator for his help in the compilation of the experimental data.

SELMA ROSEN
WILLIAM ENGLE
Microwave Lab.
ACF Electronics Div.
ACF Industries, Inc.
Paramus, N. J.

EXPERIMENTAL PROBLEM ENCOUNTERED

The experimental setup is schematized in Fig. 1. The plasma is irradiated with pulses of peak power of approximately 0.1 to 1 Mw at 5.5 Gc, a PRR of 60 and a width of 5 μ sec. The em plane wave is incident on the bottle and the full power of this wave travels through the bottle during the "formative time lag" of the gas. The gas used in our case is H₂ at a pressure of 1 mm of Hg. Following this time lag, the gas ionizes and the transmitted power is attenuated severely. The pick-up horn receives a pulse as shown in Fig. 2 where t_1 refers to the time at which the gas is ionized. This is similar to the spike and flat leakage familiar in TR tubes. The flat leakage is approximately 35-40 db below the spike. The time variation of electron density can be deduced from the instantaneous attenuation of the flat part of this signal. Thus, it is desirable to display the signal on a CRO. This was impossible to do, since the relative magnitudes of the spike power (hundreds of kilowatts) and the flat power (watts) are as shown in Fig. 2. Any attempt to observe the flat part of the transmitted signal simultaneously with the spike resulted in crystal burnout.

What is required is a component that will separate the high-power spike from the low-power flat, allowing the flat to emerge independent of the spike from a single port. The spike may then be discarded by feeding it to a high power dummy load.

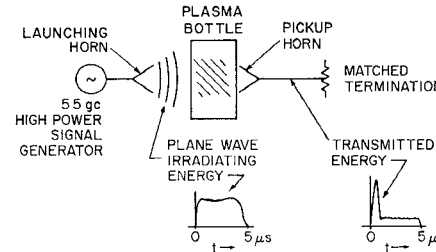


Fig. 1—Simplified schematic of plasma diagnostic experiment.

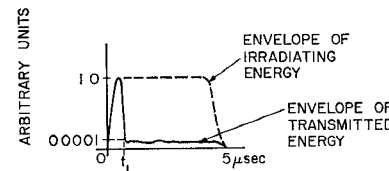


Fig. 2—Sketch illustrating the relative amplitudes of the spike and the flat portion.

USE OF SWITCH TO SEPARATE SPIKE FROM FLAT

Depicted in Fig. 3 is the additional microwave circuitry necessary to accomplish the separation of the spike and the flat portions. The critical component is the fast-acting broadband, high-peak-power switch.¹ The switch is capable of hold-off powers in excess of a megawatt at short pulse widths and, hence, its usefulness in high power

plasma diagnostics. The RF dynamic switching time is 20-30 nsec. Fig. 3 also depicts the various waveforms at the three ports of the circulator. The spike emerges at D at full peak power. The switch and associated circuitry is shown in Fig. 4.

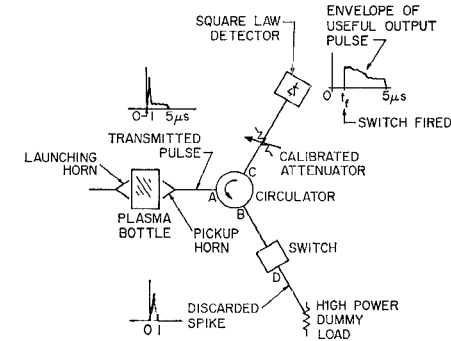
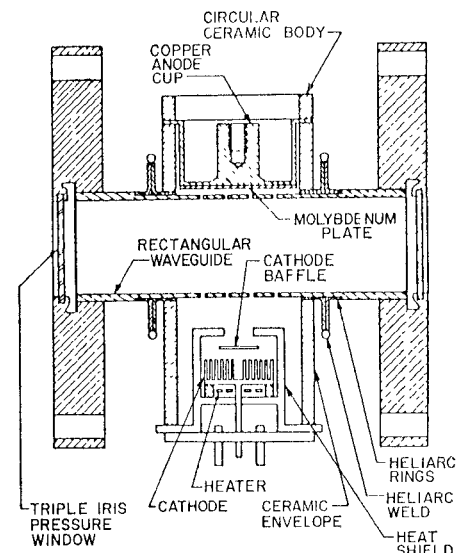
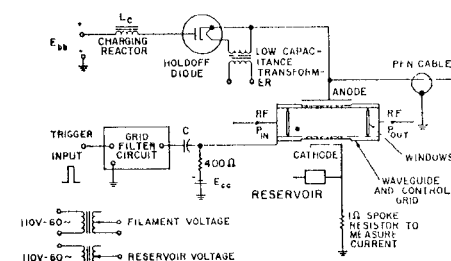


Fig. 3—Simplified schematic of improved experimental setup employing circulator and fast-acting high power switch.



THE SWITCH



THE MODULATOR

Fig. 4—The switch and associated circuitry.

The experimental arrangement operated satisfactorily. The results are best shown by the two oscilloscopes of Figs. 5 and 6. Depicted in Fig. 5 are the RF detected envelopes emerging at ports A, C and D. Peak-power levels in this oscilloscope are 140 kw. Note that the switch is fired after the spike

* Received September 16, 1963. The work reported in this communication was done while L. Lapson was a participant in the Undergraduate Science and Research Program of the National Science Foundation. The microwave switch used in this work was developed with the Rome Air Development Center, Rome, N. Y., Contract No. AF-30(602)-2135.

¹ H. Goldie, "A fast broadband high power microwave switch," *Microwave J.*, vol. VI, pp. 76-81; August, 1963.